ELSEVIER

Microelectronics Journal 35 (2004) 791–796

Microelectronics Journal

www.elsevier.com/locate/mejo

Thermal measurements of active semiconductor micro-structures acquired through the substrate using near IR thermoreflectance

James Christofferson, Ali Shakouri*

Jack Baskin School of Engineering, University of California, Santa Cruz, CA 95064, USA

Received 31 December 2003; received in revised form 29 March 2004; accepted 18 June 2004
Available online 18 August 2004

Abstract

Modern, high-density integrated circuits (IC) typically use a flip chip bonding technique to increase performance on a greater number of interconnects. In doing so, the active devices of the IC are hidden under the exposed substrate, which precludes the use of typical surface thermal characterization techniques. A near infrared thermoreflectance method is described such that the temperature of active semiconductor devices can be measured through the substrate. Experimental results were obtained through a 200 μm thick silicon substrate. Temperature resolution of 0.1 K and spatial resolution of 5 μm has been achieved. The Fabry–Perot effect, due to multiple reflections between the device and the back of the substrate, has been experimentally and theoretically analyzed. Techniques to enhance the spatial resolution will be discussed.
© 2004 Elsevier Ltd. All rights reserved.

Keywords: Thermoreflectance; Backside thermal imaging; Photothermal imaging

1. Introduction

High-resolution thermal imaging of semiconductor devices typically requires both complex experimental setup and data analysis [1–3]. Popular techniques use coatings such as liquid crystal thermography (LCT) or fluorescence micro-thermography (FMT), contact mechanical methods, such as scanning thermal microscopy (SThM), or optical techniques such as infrared (IR) microscopy, or thermoreflectance. Thermoreflectance is a well-known method [4–7] for the characterization of material parameters, or thermal mapping of active semiconductor devices. In general, a temperature increase in a solid causes a broadening and shift of the absorption edges. Through the Kramers–Kronig relation this produces a change in the index of the material and thus there is a temperature dependence of the reflection coefficient. Thermoreflectance experiments exploit this dependence to obtain a thermal distribution of active semiconductor devices. Diffraction limited spatial resolution is better than blackbody emission experiments (typically 3–5 μm) because of the use of visible light. The challenge of thermoreflectance imaging lies in resolving the weak thermoreflectance signal. Typically, for metals, the thermally induced change in the reflection coefficient are small, on the order of one part in 10^5 per degree, so for sub-degree resolution, differential measurements are performed using a lock-in technique.

Previous thermal imaging experiments have demonstrated 100 mK thermal resolution and sub-micron spatial resolution when reflecting off the top surface gold contact layer [8,9]. Now, by choosing a wavelength that is in the region of transparency of the substrate, the same thermoreflectance technique can be used to obtain thermal measurements by penetrating through the substrate and reflecting off the underside metal of the device. In developing this technique we hope to be able to measure the heating of devices in flip chip bonded integrated circuit's (IC) and other geometries, where a device is hidden under the substrate material.

2. Experiment

For a through substrate thermoreflectance measurement, a tunable (1400–1600 nm) fiber coupled laser is projected from the underside through a hole in the stage, while

* Corresponding author. Tel.: +1-831-459-3821; fax: +1-831-459-4829.
E-mail address: ali@soe.ucsc.edu (A. Shakouri).

0026-2692/$ - see front matter © 2004 Elsevier Ltd. All rights reserved.
doi:10.1016/j.mejo.2004.06.009

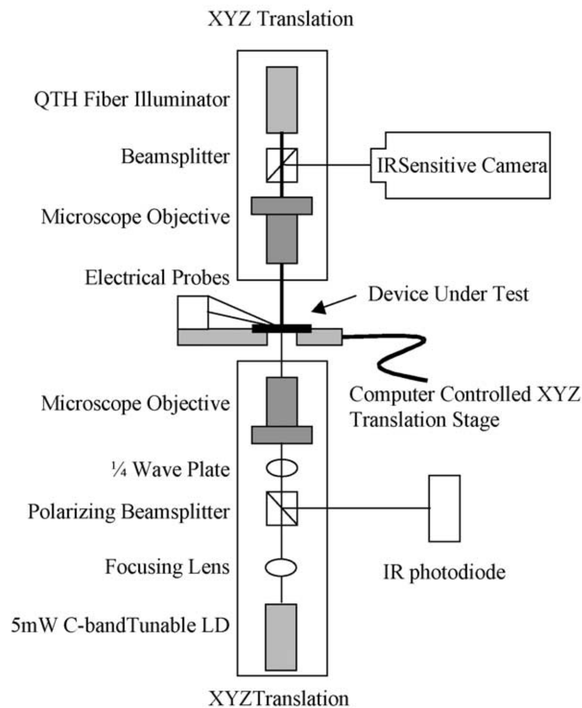

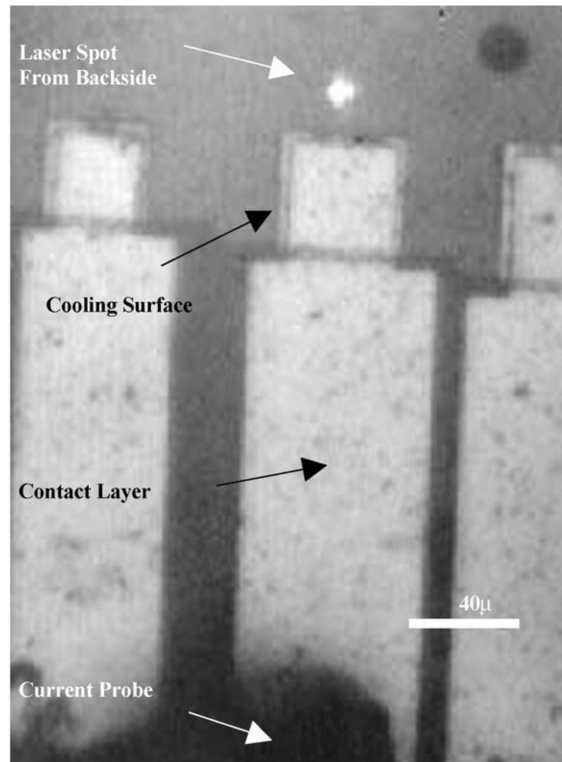

Fig. 1. Experiment setup. Image from the topside infrared sensitive camera shows a 40×40 μm micro-cooler and the 1550 nm laser spot penetrating through the substrate from the underside. The IR camera is primarily used to align the laser. After alignment, the IR camera is replaced with a visible photodiode for simultaneous topside and backside thermoreflectance scanning.

the topside is illuminated by a standard Quartz Tungsten Halogen (QTH) illuminator, as shown in Fig. 1. By using an IR sensitive camera the laser spot penetrating from the underside can be positioned to the active device under test as shown. In addition, such a configuration allows for topside thermoreflectance to be performed by replacing the topside camera with a photodiode, and lock-in amplifier. The illuminator is bright enough to project a reflected image of the region of interest, including the device under test, which is easily seen on the photodiode. By using a 100 μm pinhole, a small region corresponding to the reflected light from the device surface is selected. Thus, the temperature of the topside and underside of the device's metal layer can be measured simultaneously. A schematic of the device under test, and measurement are shown in Fig. 2. For this experiment the device under test is a 40×40 μm SiGe based micro-cooler device [10], the thermal characteristics of which have been previously studied.

3. Point measurements

A typical, calibrated [11], single point thermoreflectance measurement of device surface cooling is shown in the topside result of Fig. 3. As the bias current is increased, the Joule heating effect eventually dominates because it increases quadratically, while the Peltier cooling term only increases linearly with applied current:

$$\text{Cooling (topside measurement)} \sim \alpha I - \beta I^2$$

Where α and β are device dependent constants corresponding to the Peltier and Joule Effect, and I is the applied device

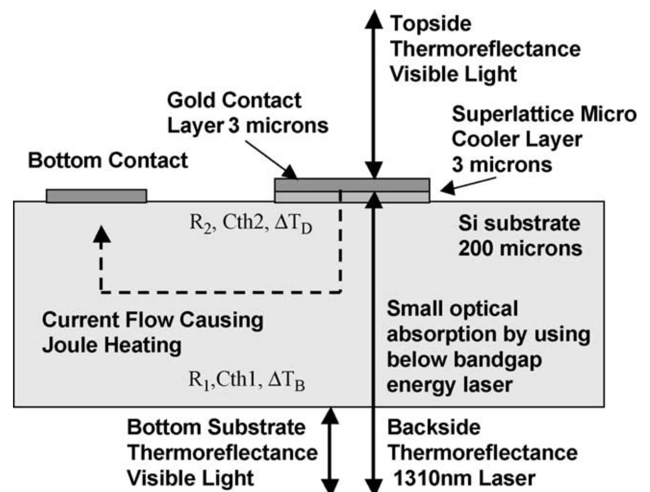

Fig. 2. Schematic of device, and measurement. R1 and R2 are the reflection off the bottom substrate and device. There is cooling at the device surface, ΔT_D and heating at the bottom of the substrate, ΔT_B. In addition there are different thermoreflectance coefficients at each reflection, Cth1, Cth2.

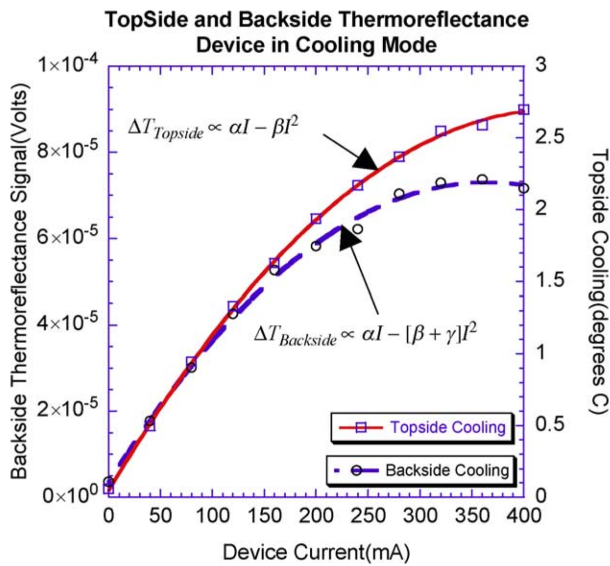

Fig. 3. Topside and underside thermoreflectance point measurement of an active micro-cooler. The measurements are not exactly the same because the underside measurement includes an extra heat source from the reflection surface off the bottom of the substrate.

current. The resulting topside measurement is as expected, which shows a maximum cooling performance of about 2.7° from the ambient room temperature.

Thermoreflectance point measurements through the substrate of the underside metal of the device, compared to the topside thermoreflectance measurement are not exactly the same even though the temperature difference on the two sides of the metal should be negligible. Because the thermoreflectance coefficient is not known for the substrate-metal reflection interface, the backside measurement is not independently calibrated to temperature, but because the peak cooling bias current has changed, as shown in Fig. 3, the measured signal cannot match the topside result by simply finding the correct coefficient. This can be explained by considering the contribution of multiple reflection surfaces when looking from the underside. Because there is also a reflection surface at the bottom of the substrate the underside signal is a combination of the device cooling and the small heating seen at the bottom substrate interface:

$$\text{Cooling (backside measurement)} \sim \alpha I - [\beta + \gamma] I^2$$

The additional Joule heating term seen from the backside is denoted γ, with the device Joule heating β and Peltier cooling term α. Visible thermoreflectance of the substrate from the backside indicates that there is only 0.1–0.2 K degrees of heating, however, this still can contribute to the backside IR measurement, mainly because there is a significant ($>30\%$) reflection off the bottom before the light enters the substrate. Even with the reflection at the bottom surface interface and the absorption in the substrate, the figure indicates that better than 0.1 K resolution was achieved over fundamental electronic noise when using a 5 μm diameter laser spot through a 200 μm substrate.

4. Fabry–Perot effects in imaging

By using a computer controlled translation, stage scanned thermal imaging is performed simultaneously on the topside and backside. Initial results have shown that the substrate cavity creates a resonance, and because the sample is not lapped exactly flat, the cavity reflection surfaces are not parallel and interference fringes emerge as the backside thermal image is acquired. Fig. 4 shows the result of a backside scan underneath the cooling surface of an active micro-cooler acquired with a fixed 1310 nm laser. Matlab simulations of the expected signal, including a small tilt angle in the bottom surface ($<0.1°$), account for the observed fringes. An image cross-section, along with the simulation result is shown in Fig. 4. The true cooling profile of the device under test as measured from the backside is contained in the amplitude envelop of these interference fringes. The fringes reduce the spatial resolution of the thermal profile.

Instead of using a fixed 1310 nm laser source, the source was replaced with a fiber coupled tunable laser, allowing for backside thermal imaging at different wavelengths. The resonant cavity mode spacing created by the substrate was

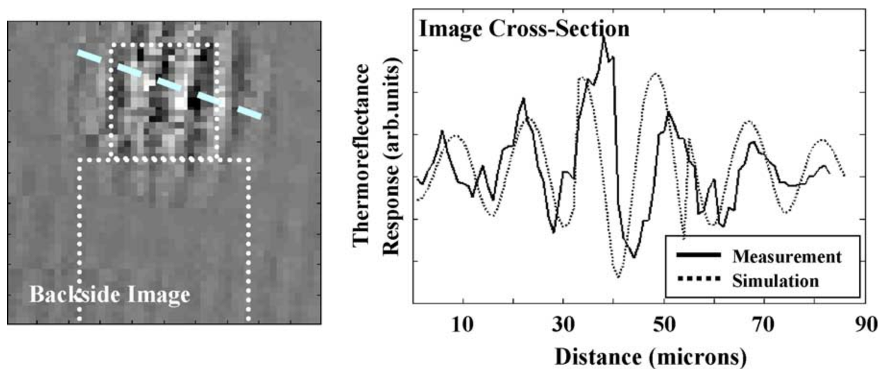

Fig. 4. Backside thermoreflectance image left, and image cross-section with simulation right. On left, the dotted line represents the approximate region of the micro-cooler while the dashed line indicates the image cross-section shown on right. The measured interference fringes (solid line) are caused by non-flat lapping of the sample and a Matlab simulation (dotted line) shows the tilt angle to be less than 0.1 degrees.

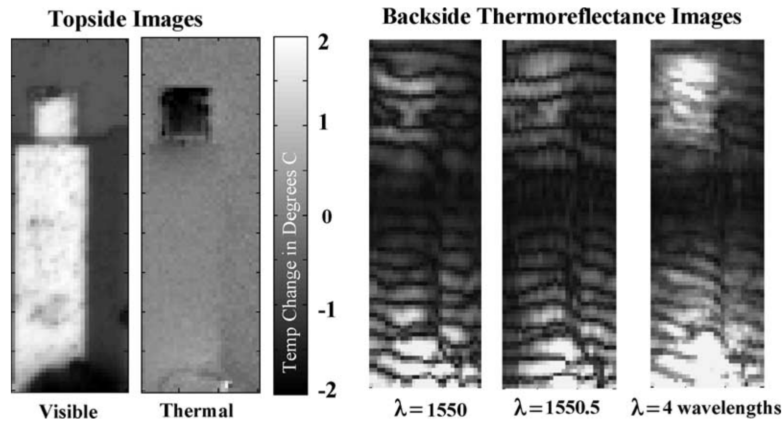

Fig. 5. Topside image, topside thermal image, backside thermoreflectance image at 1550 and 1550.5, and the first order correction. The correction is obtained by taking the maximum of the four different wavelengths backside thermoreflectance images at each pixel.

calculated to be about 2 nm apart for this wavelength. By imaging at different wavelengths, and averaging over one cavity mode, the effect of the resonance can be reduced.

Fig. 5 shows the reflection image, topside thermal image, backside images at 1550 and 1550.5 nm, and on the right, the first order image correction with the 40×40 μm micro-cooler biased to 250 mA. The image correction was obtained by taking the maximum magnitude at each point of the four wavelengths. The topside and first backside image was acquired during the same scan. There is a few microns difference in the relative position of the topside and the backside images because the alignment was done by eye. We see, in the topside thermal image, a localized cooling distribution on the top cooling surface of about 2 °C, in addition to a small amount of heating at the current probe, of about 0.5 °C. The backside image is distorted by the interference fringes, but clearly shows the cooling at the device surface and the heating underneath the probe. The scan was repeated four times and each time the wavelength of the backside laser was increased by 500 pm. The increase 500 pm was chosen because of the desire to sample one resonant mode, considering the substrate mode spacing of 2 nm.

Because the topside thermal image is acquired with the lock-in amplifier in 'X' mode, the sign of the thermal signal is retained, corresponding to heating or cooling in the thermal image. From the backside, however, the magnitude of the lock-in signal is contained in the envelope of the interference fringes, while the lock-in phase of the magnitude depends if at that point, the laser is constructively or destructively interfering. By looking at a cross-section line scan of the phase image, Fig. 6, from the current probe to the cooling surface, we can see that the periodicity of the phase signal is shifted on the contact layer, just before the device cooling surface. This is the boundary, where the heating from the current probe and the cooling from the device meet, and the temperature is zero. By determining the cross over point, from heating to cooling, contained in

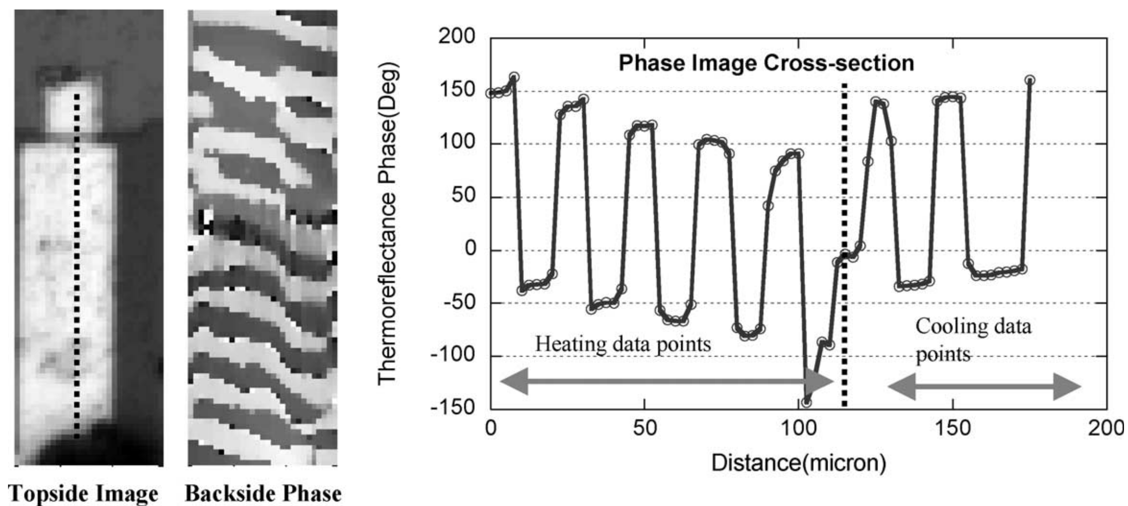

Fig. 6. Backside phase image and phase cross-section down micro-cooler for sign determination of backside thermoreflectance signal. Because of the cavity resonance the phase of the lock-in signal shows periodicity depending on constructive or destructive interference. However, a cross section of the phase image at 1550.5 nm clearly shows, where the magnitude of the signal changes sign (shifts by 180°). This indicates the boundary between the heating at the current probe and the cooling on the device surface.

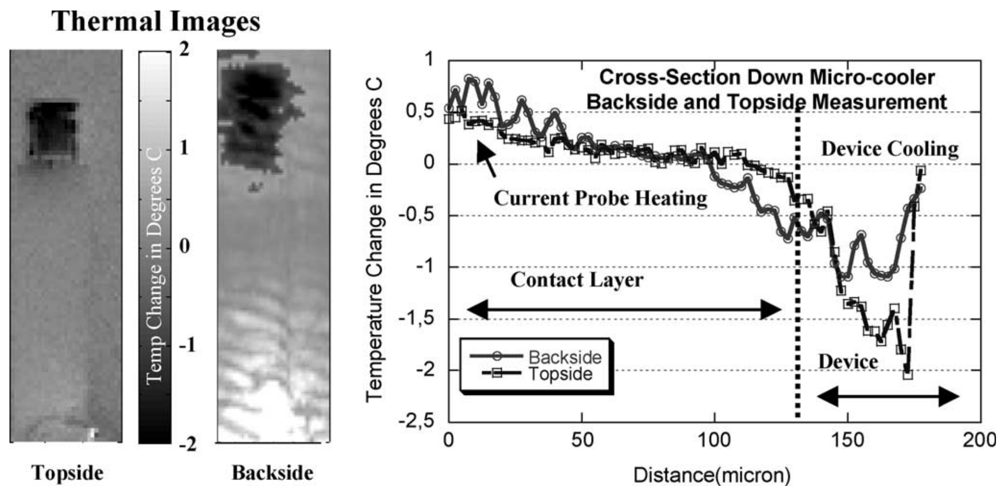

Fig. 7. Topside and backside thermal image final result. The backside image is a result of taking the maximum at each point from the series of four wavelengths and then correcting for the sign change. On right is a thermal cross-section down the micro-cooler device. With further simulation and experiment, the backside thermal image quality should approach the topside result.

the phase image, the sign of the magnitude of the backside thermal image can be corrected. The final result of image enhancement from multiple wavelengths and sign correction is shown in Fig. 7 along with a cross-section comparing the topside and backside thermal image results. The backside data was scaled to the topside data by estimating the dc reflectivity of the interfaces, loss in the cavity and the thermoreflectance coefficient of the substrate-gold interface. The measured dc value includes the reflectivity of the resonant cavity and the loss in the medium. The index and absorption depend on the doping concentration of the substrate [12], which is on the order of $10^{19}/cm^3$. Using the simulations with experimental data, the thermoreflectance coefficient at the metal-semiconductor interface is estimated to be 2×10^{-5} per degree, which is obtained assuming the temperature distribution on the metal is the same on top and bottom, and the heating on the bottom reflection surface is small. An exact value for the substrate-metal thermoreflectance coefficient is challenging because of the error in the substrate index and absorption coefficient for our highly doped device under test. More precision in the backside thermoreflectance coefficient can be obtained by obtaining experimental material parameters of the device under test rather than using published values in the simulation.

The cross sections of the topside and the backside thermal distribution down the device show the same trend, but are not exactly the same. The backside cross-section shows that the thermal signal extends beyond the cooling surface and further down the contact layer than the topside data. This is possibly due to the fact that under the contact layer is a thin layer of SiN used as an electrically insulating layer which may be effecting the thermoreflectance coefficient at this interface. More study is required to determine the detailed behavior of the thermoreflectance coefficient at the interface of substrate and metal.

5. Conclusion

Point thermal measurements and thermal images were acquired simultaneously from the topside and through the substrate of an active micro-cooler using a near IR thermoreflectance technique. The results indicate that a good signal to noise ratio can be achieved over the fundamental electronic noise, but that the interference created by the substrate cavity causes noise in the thermal image. By averaging over many wavelengths within a cavity mode created by the substrate, the spatial resolution of the backside scan can be increased. With further simulation, and experiment, the quality of backside thermal imaging should approach the topside result. The main application of this technique is for thermal imaging of flip chip bonded active IC's and other geometries, where an active device is hidden beneath the substrate.

References

[1] J. Kolzer, E. Oesterschulze, G. Deboy, Thermal imaging and measurement techniques for electronic materials and devices, Microelectronic Engineering 31 (1996) 251–270.
[2] A. Cutolo, Selected contactless optoelectronic measurements for electronic applications, Review of Scientific Instruments 69 (1998) 337–360.
[3] J. Altet, S. Dilhaire, S. Volz, J. Rampnoux, A. Rubio, S. Grauby, L. Lopez, W. Claeys, J. Saulnier, Four different approaches for the measurement of IC surface temperature: application to thermal testing, Microelectronics Journal 33 (2002) 689–696.
[4] W. Claeys, S. Dilhaire, V. Quintard, J.P. Dom, Y. Danto, Thermoreflectance optical test probe for the measurement of current-induced temperature changes in microelectronic components, Quality and Reliability Engineering International 9 (1993) 303–308.
[5] Y.S. Ju, K.E. Goodson, Short-time-scale thermal mapping of microdevices using a scanning thermoreflectance technique, Journal of Heat Transfer 120 (1998) 306.
[6] J.A. Batista, A.M. Mansanares, E.C. Da Silva, M.B.C. Pimentel, N. Jannuzzi, D. Fournier, Subsurface microscopy of biased

metal–oxide-semiconductor field-effect transistor structures: photothermal and electroreflectance images, Sensors and Actuators A 71 (1998) 40–45.

[7] S. Grauby, B.C. Forget, S. Hole, D. Fournier, High resolution photothermal imaging of high frequency phenomena using a visible charge coupled device camera associated with a multichannel lock-in scheme, Review of Scientific Instruments 70 (1999) 3603–3608.

[8] J. Christofferson, D. Vashaee, A. Shakouri, P. Melese, High resolution non-contact thermal characterization of semiconductor devices, Proceedings of the SPIE 4275 (2001) 119–125.

[9] J. Christofferson, D. Vashaee, A. Shakouri, P. Melese, X. Fan, G. Zeng, C. Labounty, J.E. Bowers, E.T. Croke, Thermoreflectance imaging of superlattice micro refrigerators, Seventeenth Annual IEEE Semiconductor Thermal Measurement and Management Symposium, San Jose, CA, 2001.

[10] A. Shakouri, J.E. Bowers, Heterostructure integrated thermionic coolers, Applied Physics Letters 71 (1997) 1234.

[11] E. Schaub, S. Dlihaire, S. Jorez, L-D. Patino Lopez, W. Claeys, Calibration procedure of temperature measurements by thermoreflectance upon microelectronic devices, International Conference on Photoacoustic and Photothermal Phenomena, Kyoto, 2000.

[12] R. Falk, Backside thermal mapping using active laser probe, Electronic Device Failure Analysis News May (2000).